A study of the ac Stark effect in doped photonic crystals

2007 J. Phys.: Condens. Matter 19 156229

(http://iopscience.iop.org/0953-8984/19/15/156229)

IOP PUBLISHING JOURNAL OF PHYSICS: CONDENSED MATTER

J. Phys.: Condens. Matter **19** (2007) 156229 (18pp) doi:10.1088/0953-8984/19/15/156229

A study of the ac Stark effect in doped photonic crystals

I Haque and Mahi R Singh

Department of Physics and Astronomy, The University of Western Ontario, London, ON, N6A 3K7, Canada

E-mail: msingh@uwo.ca

Received 10 January 2007, in final form 22 February 2007
Published 27 March 2007
Online at stacks.iop.org/JPhysCM/19/156229

Abstract

In this paper we present calculations of level populations and susceptibility for an ensemble of five-level atoms doped in a photonic crystal, using the master equation method. The atoms in the ensemble interact with the crystal which acts as a reservoir and are coupled with two strong pump fields and a weak probe field. It is found that, by manipulating the resonance energy associated with one of the decay channels of the atom, the system can be switched between an inverted and a non-inverted state. We have also observed the ac Stark effect in these atoms and have shown that due to the role played by the band structure of the photonic crystal, it is possible to switch between an absorption state and a non-absorption state of the atomic system. This is a very important finding as techniques of rendering material systems transparent to resonant laser radiation are very desirable in the fabrication of novel optical and photonic devices.

1. Introduction

Recent efforts in the study of quantum coherence and interference in quantum optics and semiconductor nanostructures have led to the discovery of many interesting phenomena [1–23]. These include lasing without inversion (LWI) [2], electromagnetically induced transparency (EIT) [3], enhancement of nonlinear susceptibility [4], the ac Stark effect [5–16, 19–23], etc. The aim of the present paper is to study the ac Stark effect in a photonic crystal doped with an ensemble of five-level nanoparticles, which leads to several new phenomena with great potential for applications. A comprehensive survey of the relevant literature suggests that this effect is yet to be investigated in this novel class of materials.

The ac Stark effect—also known as Autler–Townes (A–T) splitting—occurs due to nonlinear interactions between light and matter in the presence of one or more strong variable radiation field(s) [5]. Irradiation by a strong field leads to dynamic splitting of the energy levels of an atomic system [6]. The split states are said to be *dressed* by the strong radiation field. The splitting phenomenon is particularly well resolved when the Rabi frequency of the strong field is larger than the linewidths of the atomic energy levels [7].

Over the past three decades, the ac Stark effect has been studied—theoretically and experimentally—in many different types of systems, such as atomic gases [8, 9], laser-cooled atoms [10], ions [11], gas-phase molecules [12] and solid state materials [13], under both steady-state and transient [14] conditions. In particular, there has been considerable interest in studying the effect in three-level atoms and nanoparticles [8, 15, 16], which are taken in either of the Λ, V or Ξ (cascade or ladder) configurations.

Recently, investigations of the ac Stark effect have been extended to semiconductor nanostructures, such as quantum dots, wells, wires, etc. These nanostructures are essential for the fabrication of devices for quantum computing. Quantum dots, in particular, have been widely studied in this regard, when doped in semiconductors [17, 18]. Studies of the ac Stark effect in these structures have addressed both theoretical and experimental aspects. For example, a recent theoretical study has shown that the optical absorption spectra due to excitons in a quantum dot superlattice embedded in a nanowire exhibit ac Stark splitting [19]. On the experimental side, a similar splitting effect has been observed in the inter-subband transitions in semiconductor quantum wells and it has been shown that the dephasing mechanisms associated with these transitions have characteristics which make the wells behave as artificial atoms [20].

A type of system that has been found to be remarkably advantageous for the investigation of the diverse features of the ac Stark effect consists of a four-level atom or quantum dot driven by two pump fields and a weak probe field. At the core of this atomic configuration is a Ξ-type three-level subsystem. Wei *et al* [21] have carried out an extensive analysis of this system and found that the resulting spectrum has up to three peaks (dynamic splitting), which can be explained in terms of the dressed state formalism. Other types of four-level system that have been used in ac Stark effect studies include doubly-driven Rb and Ba atoms. For example, density matrix calculations of the fluorescence obtained from a four-level Rb atomic system have shown A–T split states and transparency effects, which have been confirmed experimentally [22]. Further empirical evidence of the effect has been found in the two-photon resonant spectrum obtained in the presence of a strong coupling field from the non-degenerate four-wave mixing in a four-level Ba system (dressed cascade configuration) [23].

The present paper, for the first time, considers the ac Stark effect in a three-dimensional photonic crystal with isotropic geometry. The crystal structure consists of an isotropic arrangement of dielectric spheres and it is doped with an ensemble of identical, non-interacting five-level atoms or quantum dots. These doped atoms interact with the photonic crystal which plays the role of a reservoir. Recently, experimental techniques have been developed for doping impurity quantum dots in photonic crystals and their optical properties have been studied [24]. These have numerous applications in quantum computing and cryptography.

The structure of a photonic crystal is achieved by a periodic arrangement of dielectric materials with differing dielectric constants [25–29]. This produces a periodicity in the dielectric constant function of the crystal which leads to the formation of energy gaps in its photon energy spectrum [25, 26], analogous to the energy gaps in the electronic band structures of semiconductors. A current major area of study involving photonic crystals focuses on the modification of radiative properties of doped atoms within the crystal reservoir [30–35].

In the calculations presented in this paper, we consider two distinct configurations of five-level atoms, driven by two strong pump fields and a weak probe field (see figure 1). Due to the interaction between the particles and the reservoir, the excited states decay spontaneously to the lower states. Expressions for the susceptibility associated with the probed transitions have been calculated using the master equation method.

Numerical simulations for the level populations and the imaginary part of the susceptibility are performed for a photonic crystal with a gap to mid-gap ratio of around 20%. It is found that by manipulating the decay rate with resonance tuning the atomic system can be switched

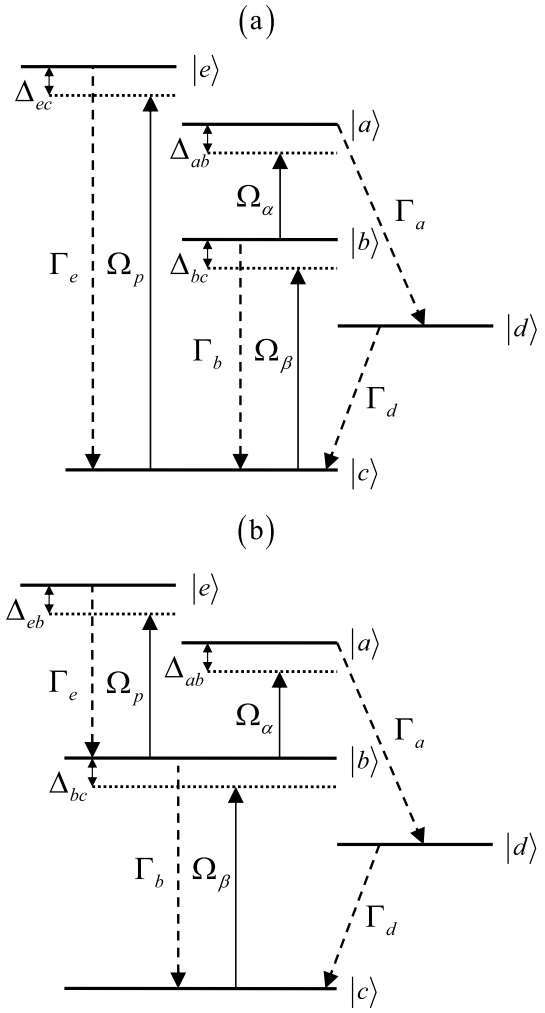

Figure 1. Schematic diagrams for the five-level atom, driven by two pump laser fields with Rabi frequencies Ω_α and Ω_β. The levels are denoted as $|a\rangle$, $|b\rangle$, $|c\rangle$, $|d\rangle$ and $|e\rangle$. The probe field with Rabi frequency Ω_p drives the (a) $|c\rangle \rightarrow |e\rangle$ or (b) $|b\rangle \rightarrow |e\rangle$ transition. The detunings of the two pump fields and the probe field are denoted as Δ_{ab}, Δ_{bc} and (a) Δ_{ec} or (b) Δ_{eb}, respectively. The dashed arrows represent the decay channels and Γ_i denotes the decay rate of level $|i\rangle$.

between an inverted and a non-inverted state, with regards to the level population of the ground state of the cascade. Furthermore, the band structure of the photonic crystal is found to have a major influence on the ac Stark effect observed in the doped atoms. In particular, the probed transition of the doped atom could be rendered transparent to any resonant radiation field, i.e. the atom can be switched between an absorption and a non-absorption state, simply by manipulating the location of the resonance energy.

2. Formulation of susceptibility

The photonic crystal is considered to be doped with an ensemble of identical, non-interacting five-level impurity atoms. The crystal structure consists of a three-dimensional isotropic

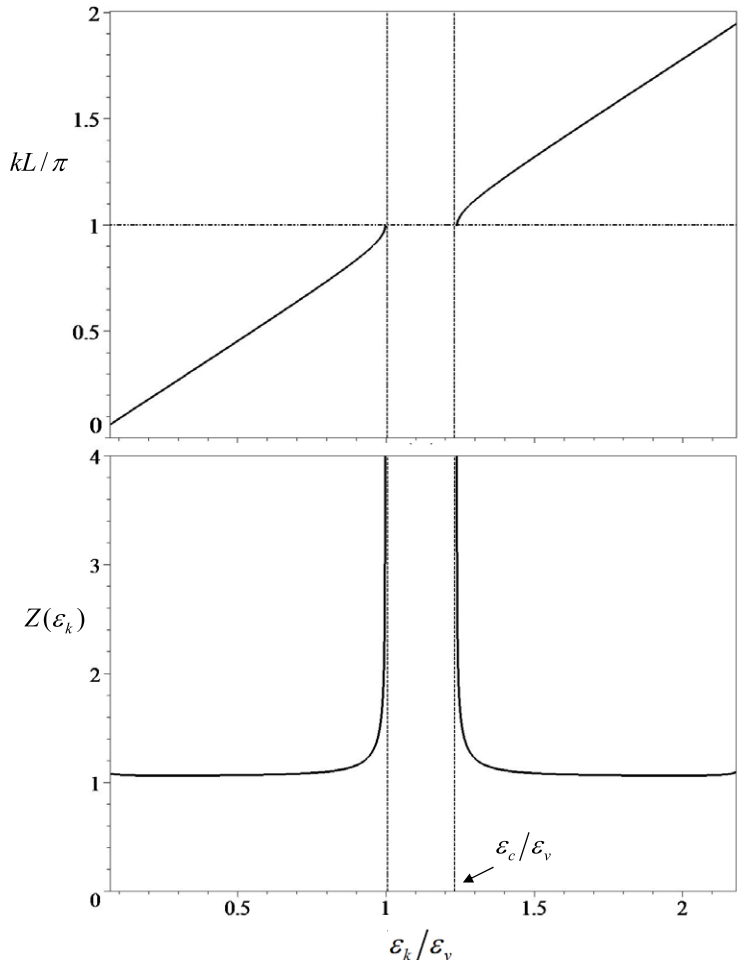

Figure 2. Plots of the dispersion relation (top panel) and the form factor $Z(\varepsilon_k)$ (bottom panel) of the photonic crystal with $n = 1.4$, $a/L = 0.2$ and $L = 300$ nm, where k denotes the wavevector. The quantities $\varepsilon_{\rm v}$ and $\varepsilon_{\rm c}$ are the maximum energy of the valence band and the minimum energy of the conduction band, respectively. The horizontal axis is the ratio of the energy ε_k to the maximum valence band energy $\varepsilon_{\rm v}$. The band gap of the crystal lies between $\varepsilon_k/\varepsilon_{\rm v} = 1$ and $\varepsilon_{\rm c}/\varepsilon_{\rm v}$, shown by the vertical dashed lines.

arrangement of dielectric spheres of radius a and refractive index n. The lattice constant of the crystal is denoted by L. The band structure equation for this particular type of photonic crystal has been calculated in [31] and can be written as:

$$\varepsilon_k = \frac{c\hbar}{4na} \arccos\left(\frac{4n\cos(kL) + (1-n)^2}{(1+n)^2}\right) \tag{1}$$

where ε_k and k denote the energies and the wavevectors of the photons, respectively, and c is the speed of light.

The energy dispersion relation given in equation (1) is plotted in figure 2 (top panel). For the given crystal parameters, the gap energy corresponds to the near infrared and the optical regions of the electromagnetic spectrum. Photonic crystals are commonly characterized by their gap to mid-gap ratio, which is defined as $2(\varepsilon_{\rm c} - \varepsilon_{\rm v})/(\varepsilon_{\rm c} + \varepsilon_{\rm v})$. For this particular crystal,

this ratio is around 20%. The parameters have been chosen to emulate the gap to mid-gap ratio obtained in Yablonovite crystals [26]. It is important to emphasize that the findings in the present paper are independent of the choice of photonic crystal.

The energy levels of an atom in the doped ensemble are denoted by $|a\rangle$, $|b\rangle$, $|c\rangle$, $|d\rangle$ and $|e\rangle$. The quantities ε_{ab}, ε_{bc} and ε_{ec} (or ε_{eb}) are the transition energies corresponding to the $|b\rangle \rightarrow |a\rangle$, $|c\rangle \rightarrow |b\rangle$ and $|c\rangle \rightarrow |e\rangle$ (or $|b\rangle \rightarrow |e\rangle$) transitions, respectively (see figure 1). The energy difference between levels $|a\rangle$ and $|d\rangle$ is denoted as ε_{ad}. For our calculations and numerical simulations it is considered that the transition energies ε_{ab}, ε_{bc} and ε_{ec} (or ε_{eb}) lie in a region away from the band gap of the photonic crystal, where its density of states (DOS) is constant and does not affect the coupling of the laser fields with the doped atoms.

We consider that the atoms in the ensemble interact with the photonic crystal reservoir. Due to this interaction, level $|a\rangle$ decays to level $|d\rangle$ and levels $|b\rangle$ and $|d\rangle$ decay to level $|c\rangle$. Level $|e\rangle$ decays to level $|c\rangle$ or level $|b\rangle$ in figures 1(a) and (b), respectively. It is important to note that the atomic arrangement described above is similar to the experimental double resonance scheme used in [36], with the exception that the present configuration has an extra level $|e\rangle$ which is used to study the absorption spectrum.

The pair of excited levels $|a\rangle$ and $|b\rangle$ and the ground level $|c\rangle$ are taken in Ξ configuration, as shown in figure 1. The transition $|b\rangle \rightarrow |a\rangle$ is driven by a strong pump laser field of energy ε_α and Rabi frequency Ω_α. Similarly, the transition $|c\rangle \rightarrow |b\rangle$ is driven by a second strong pump laser field of energy ε_β and Rabi frequency Ω_β. A weak tunable probe field of energy ε_p and electric field amplitude E_p is applied between the ground level $|c\rangle$ (or the middle level $|b\rangle$) and another excited level $|e\rangle$, as seen in figure 1(a) (or 1(b)). This weak field facilitates the study of the absorption spectrum of the atom. Other transitions are dipole forbidden. It is important to note that this type of atomic configuration has been previously used in [21]. A significant difference is that our model has a fifth level $|d\rangle$ which acts as the base level in the decay channel originating from the excited level $|a\rangle$. The addition of this extra level produces very interesting results which are used to propose new switching techniques. These are discussed in the next section.

The Hamiltonian of the system, for the configuration in figure 1(a), is written in energy space as

$$H = H_\mathrm{A} + V_{\mathrm{A-F}} + H_\mathrm{R} + V_{\mathrm{A-R}} \tag{2}$$

where

$$H_\mathrm{A} = \varepsilon_a\sigma_{aa} + \varepsilon_b\sigma_{bb} + \varepsilon_\mathrm{c}\sigma_{cc} + \varepsilon_d\sigma_{dd} + \varepsilon_e\sigma_{ee} \tag{3a}$$

$$V_{\mathrm{A-F}} = -(\hbar/2)(\Omega_\alpha\sigma_{ab}^{+}\mathrm{e}^{-\mathrm{i}(\varepsilon_\alpha-\varepsilon_{ab})t/\hbar} + \Omega_\beta\sigma_{bc}^{+}\mathrm{e}^{-\mathrm{i}(\varepsilon_\beta-\varepsilon_{bc})t/\hbar} + \Omega_\mathrm{p}\sigma_{ec}^{+}\mathrm{e}^{-\mathrm{i}(\varepsilon_\mathrm{p}-\varepsilon_{ec})t/\hbar}) + \mathrm{h.c.} \tag{3b}$$

$$H_\mathrm{R} = \int_C \frac{\mathrm{d}\varepsilon_k}{2\pi}\varepsilon_k p^{+}(\varepsilon_k)p(\varepsilon_k) \tag{3c}$$

$$\begin{aligned} V_{\mathrm{A-R}} = &-\int_C \frac{\mathrm{d}\varepsilon_k}{2\pi}\sqrt{\gamma_0}Z(\varepsilon_k)p(\varepsilon_k)\sigma_{ad}^{+}\mathrm{e}^{-\mathrm{i}(\varepsilon_k-\varepsilon_{ad})t/\hbar} \\ &- \sum_{i=b,d}\int_C \frac{\mathrm{d}\varepsilon_{k'}}{2\pi}\sqrt{\gamma_0}Z(\varepsilon_{k'})p(\varepsilon_{k'})\sigma_{ic}^{+}\mathrm{e}^{-\mathrm{i}(\varepsilon_{k'}-\varepsilon_{ic})t/\hbar} \\ &- \int_C \frac{\mathrm{d}\varepsilon_{k''}}{2\pi}\sqrt{\gamma_0}Z(\varepsilon_{k''})p(\varepsilon_{k''})\sigma_{ec}^{+}\mathrm{e}^{-\mathrm{i}(\varepsilon_{k''}-\varepsilon_{ec})t/\hbar} + \mathrm{h.c.} \end{aligned} \tag{3d}$$

In the above, ε_i denotes the energy of level $|i\rangle$ and $\varepsilon_{ij} = \varepsilon_i - \varepsilon_j$. The operators $\sigma_{ii} = |i\rangle\langle i|$ and $\sigma_{ij}^{+} = |i\rangle\langle j|$, where $|i\rangle$ and $|j\rangle$ denote levels $|a\rangle$, $|b\rangle$, $|c\rangle$, $|d\rangle$ and $|e\rangle$. In equation (2), H_A, $V_{\mathrm{A-F}}$, H_R and $V_{\mathrm{A-R}}$ are the Hamiltonians of the five-level atom, the atom–field interactions, the crystal reservoir and the atom–reservoir interaction, respectively. The interaction Hamiltonians

$V_{\mathrm{A-F}}$ and $V_{\mathrm{A-R}}$ given in equations (3*b*) and (3*d*) are obtained under the electric dipole and rotating wave approximations [31]. The $p(\varepsilon_k)$ and $p^{\dagger}(\varepsilon_k)$ operators denote the annihilation and creation of photons, respectively, where ε_k is the band structure energy defined in equation (1). The integration contour C consists of two intervals: $-\infty < \varepsilon_k \leqslant \varepsilon_{\mathrm{v}}$ and $\varepsilon_{\mathrm{c}} \leqslant \varepsilon_k < \infty$. The quantity γ_0 is the vacuum decay rate, as defined in [33]. All frequencies discussed in this paper are measured with respect to γ_0. Note that the Hamiltonian for the atom in figure 1(b) can be written as in equation (2) with σ_{ec}^{+}, ε_{ec} and ε_{ic} in equations (3*b*) and (3*d*) replaced by σ_{eb}^{+}, ε_{eb} and ε_{ib}, respectively.

$Z(\varepsilon_k)$ is the form factor which is derived from equation (1) and is written as [32]:

$$Z(\varepsilon_k) = \frac{\left[4n(a/L)(1+n)^2 \sin(4na\varepsilon_k/c\hbar)\right]^{1/2}}{\left[16n^2 - \left[(1+n)^2 \cos(4na\varepsilon_k/c\hbar) - (1-n)^2\right]^2\right]^{1/4}}. \tag{4}$$

Note that the form factor, plotted in the bottom panel of figure 2, depends on the refractive index n and the ratio a/L. Also of note is the fact that it has a constant value of almost unity when ε_k is away from the band gap and a very large value when ε_k lies near either of the band edges.

It is important to emphasize that, in the present paper, we have considered an isotropic photonic crystal. The difference between an isotropic and an anisotropic crystal is that the former has a band gap which is identical in all directions whereas the latter's band gap is direction-dependent. The band structure of an anisotropic photonic crystal as seen from the point of view of a doped particle varies with its location. The form factor given in equation (4) depends on the DOS which is determined by the energy gap of the crystal. As a result, the form factor for an anisotropic crystal has anisotropic values in different crystal directions. The predictions made in the present paper using the band structure of an isotropic crystal are valid for all types of photonic crystals which have energy gaps in their dispersion relations.

The aim of this section is to obtain an expression for the susceptibility due to the weak probe field. For the case of the atom in figure 1(a), the susceptibility can be written as [37]:

$$\chi_1 = \frac{2\mu_{ec}\rho_{ec}}{\epsilon_0 E_{\mathrm{p}}} \tag{5}$$

where ρ_{ij} and μ_{ij} denote the elements of the density matrix and the dipole operator associated with the transition $|j\rangle \rightarrow |i\rangle$, respectively, and ϵ_0 is the dielectric constant of the medium. The density matrix elements can be calculated using the master equation method.

The system is prepared in such a way that initially the atoms are in ground state $|c\rangle$. As the pump fields are switched on, the excited levels become populated. Using equations (2) and (3) and following the method used in [21, 34, 35, 37], the equations of motion of the density matrix elements can be written as follows:

$$\dot{\rho}_{aa} = -\Gamma_a \rho_{aa} - \mathrm{i}\Omega_\alpha(\rho_{ab} - \rho_{ba})/2 \tag{6a}$$

$$\dot{\rho}_{bb} = -\Gamma_b \rho_{bb} + \mathrm{i}[\Omega_\alpha(\rho_{ab} - \rho_{ba}) - \Omega_\beta(\rho_{bc} - \rho_{cb})]/2 \tag{6b}$$

$$\dot{\rho}_{cc} = \Gamma_b \rho_{bb} + \Gamma_d \rho_{dd} + \Gamma_e \rho_{ee} + \mathrm{i}[\Omega_\beta(\rho_{bc} - \rho_{cb}) + \Omega_{\mathrm{p}}(\rho_{ec} - \rho_{ce})]/2 \tag{6c}$$

$$\dot{\rho}_{dd} = \Gamma_a \rho_{aa} - \Gamma_d \rho_{dd} \tag{6d}$$

$$\dot{\rho}_{ee} = -\Gamma_e \rho_{ee} - \mathrm{i}\Omega_{\mathrm{p}}(\rho_{ec} - \rho_{ce})/2 \tag{6e}$$

$$\dot{\rho}_{ab} = [\mathrm{i}\Delta_{ab} - \Gamma_{ab}]\rho_{ab} - \mathrm{i}[\Omega_\alpha(\rho_{aa} - \rho_{bb}) + \Omega_\beta \rho_{ac}]/2 \tag{6f}$$

$$\dot{\rho}_{ac} = [\mathrm{i}(\Delta_{ab} + \Delta_{bc}) - \Gamma_a/2]\rho_{ac} + \mathrm{i}[\Omega_\alpha \rho_{bc} - \Omega_\beta \rho_{ab} - \Omega_{\mathrm{p}} \rho_{ae}]/2 \tag{6g}$$

$$\dot{\rho}_{ad} = [\mathrm{i}(\Delta_{ab} + \Delta_{bc}) - \Gamma_{ad}]\rho_{ad} + \mathrm{i}\Omega_\alpha \rho_{bd}/2 \tag{6h}$$

$$\dot{\rho}_{bc} = [\mathrm{i}\Delta_{bc} - \Gamma_b/2]\rho_{bc} + \mathrm{i}[\Omega_\alpha \rho_{ac} - \Omega_\beta(\rho_{bb} - \rho_{cc}) - \Omega_{\mathrm{p}} \rho_{be}]/2 \tag{6i}$$

$$\dot{\rho}_{bd} = [\mathrm{i}\Delta_{bc} - \Gamma_{bd}]\rho_{bd} + \mathrm{i}[\Omega_\alpha \rho_{ad} + \Omega_\beta \rho_{cd}]/2 \tag{6j}$$
$$\dot{\rho}_{dc} = -\Gamma_d \rho_{dc}/2 - \mathrm{i}[\Omega_\beta \rho_{db} + \Omega_\mathrm{p} \rho_{de}]/2 \tag{6k}$$
$$\dot{\rho}_{ea} = [\mathrm{i}(\Delta_{ec} - \Delta_{ab} - \Delta_{bc}) - \Gamma_{ae}]\rho_{ea} - \mathrm{i}[\Omega_\alpha \rho_{eb} - \Omega_\mathrm{p} \rho_{ca}]/2 \tag{6l}$$
$$\dot{\rho}_{eb} = [\mathrm{i}(\Delta_{ec} - \Delta_{bc}) - \Gamma_{be}]\rho_{eb} - \mathrm{i}[\Omega_\alpha \rho_{ea} + \Omega_\beta \rho_{ec} - \Omega_\mathrm{p} \rho_{cb}]/2 \tag{6m}$$
$$\dot{\rho}_{ec} = [\mathrm{i}\Delta_{ec} - \Gamma_e/2]\rho_{ec} - \mathrm{i}[\Omega_\beta \rho_{eb} - \Omega_\mathrm{p}(\rho_{cc} - \rho_{ee})]/2 \tag{6n}$$
$$\dot{\rho}_{ed} = [\mathrm{i}\Delta_{ec} - \Gamma_{de}]\rho_{ed} + \mathrm{i}\Omega_\mathrm{p} \rho_{cd}/2 \tag{6o}$$

where $\Gamma_{ij} = (\Gamma_i + \Gamma_j)/2$ and the Rabi frequency $\Omega_\mathrm{p} = \mu_{ec} E_\mathrm{p}/2\hbar$. The real detuning terms appearing in the differential equations in equation (6) are given by $\Delta_{ab} = (\varepsilon_\alpha - \varepsilon_{ab})/\hbar$, $\Delta_{bc} = (\varepsilon_\beta - \varepsilon_{bc})/\hbar$ and $\Delta_{ec} = (\varepsilon_\mathrm{p} - \varepsilon_{ec})/\hbar$.

The Γ_i terms in the density matrix equations are the reservoir-mediated decay rates. These are obtained, assuming that the resonance energies lie within the bands of the photonic crystal [33], from:

$$\Gamma_a = \gamma_0 Z(\varepsilon_{ad})^2, \qquad \Gamma_b = \gamma_0 Z(\varepsilon_{bc})^2 \tag{7a}$$
$$\Gamma_d = \gamma_0 Z(\varepsilon_{dc})^2, \qquad \Gamma_e = \gamma_0 Z(\varepsilon_{ec})^2. \tag{7b}$$

It has been shown that when the resonance energy lies within the band gap, $\Gamma_i = 0$ [33].

The density matrix element ρ_{ec} has been calculated, under the steady-state approximation in the first order of the Rabi frequency Ω_p, using the method in [21]. The calculation includes all orders of the pump field Rabi frequencies Ω_α and Ω_β. The susceptibility, which is a complex quantity, is written as $\chi_1 = \chi_1' + \mathrm{i}\chi_1''$ with χ_1' and χ_1'' denoting the real and imaginary parts, respectively. Using the definition in equation (5), χ_1' and χ_1'' can be expressed as follow:

$$\chi_1' = \frac{\chi_0(G_1' H_1' + G_1'' H_1'')}{(H_1')^2 + (H_1'')^2} \tag{8a}$$
$$\chi_1'' = \frac{\chi_0(G_1'' H_1' - G_1' H_1'')}{(H_1')^2 + (H_1'')^2} \tag{8b}$$

where $\chi_0 = \mu_{ec}^2/(\epsilon_0 \hbar \gamma_0)$.

The terms G_1', G_1'', H_1', and H_1'' appearing in equation (8) are real-valued and are given by

$$G_1' = -\Omega_\beta(\Delta_{ea} P_{cb}' + \Gamma_{ae} P_{cb}'' + \Omega_\alpha P_{ca}''/2)/2 - \rho_{cc}^{(0)}(\Gamma_{be}\Delta_{ea} + \Gamma_{ae}\Delta_{eb}) \tag{9a}$$
$$G_1'' = \Omega_\beta(\Delta_{ea} P_{cb}'' - \Gamma_{ae} P_{cb}' + \Omega_\alpha P_{ca}'/2)/2 - \rho_{cc}^{(0)}(\Gamma_{ae}\Gamma_{be} + \Omega_\alpha^2/4 - \Delta_{ea}\Delta_{eb}) \tag{9b}$$
$$H_1' = \Delta_{ec}(\Gamma_{be}\Delta_{ea} + \Gamma_{ae}\Delta_{eb}) - \Gamma_e(\Gamma_{ae}\Gamma_{be} - \Delta_{ea}\Delta_{eb})/2 - (\Gamma_{ae}\Omega_\beta^2/4 + \Gamma_e\Omega_\alpha^2/2) \tag{9c}$$
$$H_1'' = \Delta_{ec}(\Gamma_{ae}\Gamma_{be} - \Delta_{ea}\Delta_{eb}) + \Gamma_e(\Gamma_{be}\Delta_{ea} + \Gamma_{ae}\Delta_{eb})/2 + (\Delta_{ea}\Omega_\beta^2/4 + \Gamma_e\Omega_\alpha^2/2) \tag{9d}$$

where the detuning terms are defined as $\Delta_{ea} = \Delta_{ec} - \Delta_{ab} - \Delta_{bc}$ and $\Delta_{eb} = \Delta_{ec} - \Delta_{bc}$.

The P_{cb}', P_{cb}'', P_{ca}' and P_{ca}'' terms in equations (9*a*) and (9*b*) have been derived as follows:

$$\begin{aligned} P_{cb}' &= X_{cb}'\rho_{bb}^{(0)} + Y_{cb}'\rho_{aa}^{(0)} + S_{cb}'\rho_{dd}^{(0)} + Z_{cb}', \\ P_{cb}'' &= X_{cb}''\rho_{bb}^{(0)} + Y_{cb}''\rho_{aa}^{(0)} + S_{cb}''\rho_{dd}^{(0)} + Z_{cb}'' \end{aligned} \tag{10a}$$
$$\begin{aligned} P_{ca}' &= X_{ca}'\rho_{bb}^{(0)} + Y_{ca}'\rho_{aa}^{(0)} + S_{ca}'\rho_{dd}^{(0)} + Z_{ca}', \\ P_{ca}'' &= X_{ca}''\rho_{bb}^{(0)} + Y_{ca}''\rho_{aa}^{(0)} + S_{ca}''\rho_{dd}^{(0)} + Z_{ca}'' \end{aligned} \tag{10b}$$

where the zeroth-order density matrix elements $\rho_{aa}^{(0)}$, $\rho_{bb}^{(0)}$ and $\rho_{dd}^{(0)}$ appearing in equations (9) and (10) are written as:

$$\begin{aligned}
\rho_{aa}^{(0)} &= \Omega_\alpha^2(X_{aa}\rho_{bb}^{(0)} + Z_{aa})/2 \\
\rho_{dd}^{(0)} &= [\Gamma_a\Omega_\alpha^2(X_{aa}\rho_{bb}^{(0)} + Z_{aa})]/2\Gamma_d \\
\rho_{bb}^{(0)} &= \frac{\Omega_\alpha^2 Z_{aa}[\Omega_\beta^2(\Gamma_d\,\mathrm{Re}(Y_{bc}) + \Gamma_a\,\mathrm{Re}(S_{bc}))/2 - \Gamma_a]/2 + \Omega_\beta^2\Gamma_d\,\mathrm{Re}(Z_{bc})/2}{\Gamma_d[\Gamma_b - \Omega_\beta^2\,\mathrm{Re}(X_{bc})/2] - \Omega_\alpha^2 X_{aa}[\Omega_\beta^2(\Gamma_d\,\mathrm{Re}(Y_{bc}) + \Gamma_a\,\mathrm{Re}(S_{bc}))/2 - \Gamma_a]/2}
\end{aligned} \tag{11}$$

with

$$X_{aa} = \frac{\Gamma_d X'_{ab}}{\Gamma_d\Gamma_a - \Omega_\alpha^2\left[\Gamma_d Y'_{ab} + \Gamma_a S'_{ab}\right]/2}, \qquad Z_{aa} = \frac{\Gamma_d Z'_{ab}}{\Gamma_d\Gamma_a - \Omega_\alpha^2\left[\Gamma_d Y'_{ab} + \Gamma_a S'_{ab}\right]/2}. \tag{12}$$

The density matrix element $\rho_{cc}^{(0)}$ is obtained from $\rho_{cc}^{(0)} = 1 - \rho_{aa}^{(0)} - \rho_{bb}^{(0)} - \rho_{dd}^{(0)}$.

The complex-valued terms $X_{ij} = X'_{ij} + \mathrm{i}X''_{ij}$, $Y_{ij} = Y'_{ij} + \mathrm{i}Y''_{ij}$, $Z_{ij} = Z'_{ij} + \mathrm{i}Z''_{ij}$ and $S_{ij} = S'_{ij} + \mathrm{i}S''_{ij}$ appearing in equations (10)–(12) are derived as:

$$\begin{aligned}
X_{ab} &= \frac{-d_{bc}d_{ac} + \Omega_\beta^2/2 - \Omega_\alpha^2/4}{D}, \qquad X_{ca} = \frac{2d_{ba} + d_{cb}}{D}, \\
X_{cb} &= \frac{2d_{ca}d_{ba} + \Omega_\beta^2/2 - \Omega_\alpha^2/4}{D} \\
Y_{ab} &= \frac{d_{bc}d_{ac} + \Omega_\alpha^2/4 + \Omega_\beta^2/4}{D}, \qquad Y_{ca} = \frac{d_{ba} - d_{cb}}{D}, \\
Y_{cb} &= \frac{d_{ca}d_{ba} + \Omega_\alpha^2/4 + \Omega_\beta^2/4}{D} \\
Z_{ab} &= -\frac{\Omega_\beta^2}{4D} = -S_{ab}, \qquad Z_{ca} = -\frac{d_{ba}}{D} = -S_{ca}, \\
Z_{cb} &= \frac{-d_{ca}d_{ba} + \Omega_\beta^2/4}{D} = -S_{cb}
\end{aligned} \tag{13}$$

with

$$D = d_{cb}d_{ba}d_{ca} + d_{ba}\Omega_\alpha^2/4 + d_{cb}\Omega_\beta^2/4 \tag{14}$$

where $d_{ij} = \mathrm{i}\Delta_{ij} - \Gamma_{ij}$, which denotes the complex detuning of the laser field coupled to the transition $|i\rangle \rightarrow |j\rangle$.

Similar calculations have also been performed for the atom in figure 1(b), where the weak field probes the $|b\rangle \rightarrow |e\rangle$ transition. The corresponding equations of motion of the density matrix elements are written as:

$$\dot{\rho}_{aa} = -\Gamma_a\rho_{aa} - \mathrm{i}\Omega_\alpha(\rho_{ab} - \rho_{ba})/2 \tag{15a}$$

$$\dot{\rho}_{bb} = -\Gamma_b\rho_{bb} + \Gamma_e\rho_{ee} + \mathrm{i}[\Omega_\alpha(\rho_{ab} - \rho_{ba}) - \Omega_\beta(\rho_{bc} - \rho_{cb}) + \Omega_\mathrm{p}(\rho_{eb} - \rho_{be})]/2 \tag{15b}$$

$$\dot{\rho}_{cc} = \Gamma_b\rho_{bb} + \Gamma_d\rho_{dd} + \mathrm{i}\Omega_\beta(\rho_{bc} - \rho_{cb})/2 \tag{15c}$$

$$\dot{\rho}_{dd} = \Gamma_a\rho_{aa} - \Gamma_d\rho_{dd} \tag{15d}$$

$$\dot{\rho}_{ee} = -\Gamma_e\rho_{ee} - \mathrm{i}\Omega_\mathrm{p}(\rho_{eb} - \rho_{be})/2 \tag{15e}$$

$$\dot{\rho}_{ab} = [\mathrm{i}\Delta_{ab} - \Gamma_{ab}]\rho_{ab} - \mathrm{i}[\Omega_\alpha(\rho_{aa} - \rho_{bb}) + \Omega_\beta\rho_{ac} + \Omega_\mathrm{p}\rho_{ae}]/2 \tag{15f}$$

$$\dot{\rho}_{ac} = [\mathrm{i}(\Delta_{ab} + \Delta_{bc}) - \Gamma_a/2]\rho_{ac} + \mathrm{i}[\Omega_\alpha\rho_{bc} - \Omega_\beta\rho_{ab}]/2 \tag{15g}$$

$$\dot{\rho}_{ad} = [\mathrm{i}(\Delta_{ab} + \Delta_{bc}) - \Gamma_{ad}]\rho_{ad} + \mathrm{i}\Omega_\alpha\rho_{bd}/2 \tag{15h}$$

$$\dot{\rho}_{bc} = [\mathrm{i}\Delta_{bc} - \Gamma_b/2]\rho_{bc} + \mathrm{i}[\Omega_\alpha\rho_{ac} - \Omega_\beta(\rho_{bb} - \rho_{cc}) + \Omega_\mathrm{p}\rho_{ec}]/2 \tag{15i}$$

$$\dot{\rho}_{bd} = [\mathrm{i}\Delta_{bc} - \Gamma_{bd}]\rho_{bd} + \mathrm{i}[\Omega_\alpha\rho_{ad} + \Omega_\beta\rho_{cd} + \Omega_\mathrm{p}\rho_{ed}]/2 \tag{15j}$$

$$\dot{\rho}_{dc} = -\Gamma_d \rho_{dc}/2 - \mathrm{i}\Omega_\beta \rho_{db}/2 \tag{15k}$$

$$\dot{\rho}_{ea} = [\mathrm{i}(\Delta_{eb} - \Delta_{ab}) - \Gamma_{ae}]\rho_{ea} - \mathrm{i}[\Omega_\alpha \rho_{eb} - \Omega_\mathrm{p}\rho_{ba}]/2 \tag{15l}$$

$$\dot{\rho}_{eb} = [\mathrm{i}\Delta_{eb} - \Gamma_{be}]\rho_{eb} - \mathrm{i}[\Omega_\alpha \rho_{ea} + \Omega_\beta \rho_{ec} + \Omega_\mathrm{p}(\rho_{ee} - \rho_{bb})]/2 \tag{15m}$$

$$\dot{\rho}_{ec} = [\mathrm{i}(\Delta_{eb} + \Delta_{bc}) - \Gamma_e/2]\rho_{ec} - \mathrm{i}[\Omega_\beta \rho_{eb} - \Omega_\mathrm{p}\rho_{bc}]/2 \tag{15n}$$

$$\dot{\rho}_{ed} = [\mathrm{i}(\Delta_{eb} + \Delta_{bc}) - \Gamma_{de}]\rho_{ed} + \mathrm{i}\Omega_\mathrm{p}\rho_{bd}/2 \tag{15o}$$

where the decay rate $\Gamma_e = \gamma_0 Z(\varepsilon_{eb})^2$, the modified probe field detuning $\Delta_{eb} = (\varepsilon_\mathrm{p} - \varepsilon_{eb})/\hbar$ and the Rabi frequency $\Omega_\mathrm{p} = \mu_{eb}E_\mathrm{p}/2\hbar$. Apart from these exceptions, all other quantities are defined as for the previous atomic configuration. In this case, we can write the real and imaginary parts of the susceptibility as:

$$\chi_2' = \frac{\chi_0(G_2'H_1' + G_2''H_1'')}{(H_1')^2 + (H_1'')^2} \tag{16a}$$

$$\chi_2'' = \frac{\chi_0(G_2''H_1' - G_2'H_1'')}{(H_1')^2 + (H_1'')^2} \tag{16b}$$

where it has been assumed that $\mu_{eb} = \mu_{ec}$.

The real-valued terms G_2' and G_2'' appearing in equation (16) are given by

$$G_2' = \Omega_\beta(\Delta_{ea}P_{cb}'' - \Gamma_{ae}P_{cb}')/2 - \Omega_\alpha(\Gamma_e P_{ab}'/2 + \Delta_{ec}P_{ab}'')/2 - \rho_{cc}^{(0)}(\Gamma_e\Delta_{ea}/2 + \Gamma_{ae}\Delta_{ec}) \tag{17a}$$

$$G_2'' = \Omega_\beta(\Delta_{ea}P_{cb}' + \Gamma_{ae}P_{cb}'')/2 + \Omega_\alpha(\Gamma_e P_{ab}''/2 + \Delta_{ec}P_{ab}')/2 - \rho_{cc}^{(0)}(\Gamma_e\Gamma_{ae}/2 - \Delta_{ea}\Delta_{ec}) \tag{17b}$$

where

$$\begin{aligned} P_{ab}' &= X_{ab}'\rho_{bb}^{(0)} + Y_{ab}'\rho_{aa}^{(0)} + S_{ab}'\rho_{dd}^{(0)} + Z_{ab}', \\ P_{ab}'' &= X_{ab}''\rho_{bb}^{(0)} + Y_{ab}''\rho_{aa}^{(0)} + S_{ab}''\rho_{dd}^{(0)} + Z_{ab}'' \end{aligned} \tag{18}$$

The detuning terms in this case are given by $\Delta_{ec} = \Delta_{eb} + \Delta_{bc}$ and $\Delta_{ea} = \Delta_{eb} - \Delta_{ab}$. The complex-valued terms X_{ab}, Y_{ab}, Z_{ab} and S_{ab} are identical to those in the case of the first atom. The density matrix elements $\rho_{aa}^{(0)}$, $\rho_{bb}^{(0)}$, $\rho_{cc}^{(0)}$ and $\rho_{dd}^{(0)}$ appearing in equations (17) and (18) are also as defined before.

3. Results and discussions

In this section we present numerical simulations of the density matrix elements and the imaginary part of the susceptibility for the isotropic photonic crystal discussed in the previous section.

First we calculate the time evolution of the level populations of the doped atoms. Our primary aim is to study the effect of the band structure of the crystal reservoir on the population densities of the atomic energy levels. The differential equations for the density matrix elements given in (6) are solved numerically, using a Fehlberg fourth–fifth-order Runge–Kutta method in the Maple scientific computing environment. As an initial condition, it is assumed that $\rho_{cc}(0) = 1$ and all other levels are unpopulated.

The numerical solutions are obtained for the atomic scheme in figure 1(a) and are shown in figure 3. The two pump laser fields are considered to be resonant, i.e. $\Delta_{ab}/\gamma_0 = \Delta_{bc}/\gamma_0 = 0$, and the detuning of the probe field $\Delta_{ec}/\gamma_0 = 10$. The Rabi frequencies of the pump and probe fields are taken as $\Omega_\alpha/\gamma_0 = \Omega_\beta/\gamma_0 = 2$ and $\Omega_\mathrm{p}/\gamma_0 = 0.2$. Note that similar parameters have been used in [21]. The plots in figures 3(a)–(c) and (d) show the population densities ρ_{aa}, ρ_{dd}, ρ_{bb} and ρ_{cc}, respectively. The solid and dotted curves in these figures represent the cases where

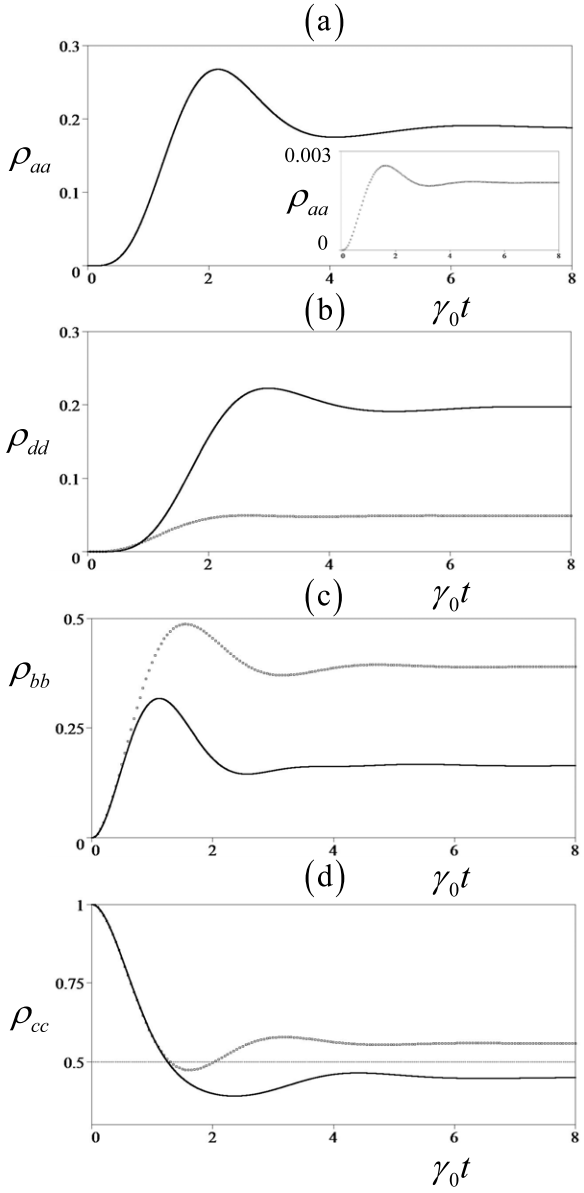

Figure 3. Numerical plots of the time evolution of the population densities (a) ρ_{aa}, (b) ρ_{dd}, (c) ρ_{bb} and (d) ρ_{cc} of the atom in figure 1(a). The horizontal axes show dimensionless time $\gamma_0 t$. The solid curves are drawn for the case where $\varepsilon_{ad}/\varepsilon_{\mathrm{v}} = 80.00\%$. The dotted curves represent the case where $\varepsilon_{ad}/\varepsilon_{\mathrm{v}} = 99.99\%$. All other resonance energies are kept far from either of the band edges.

the resonance energy ε_{ad} is away from ($\varepsilon_{ad}/\varepsilon_{\mathrm{v}} = 80.00\%$) and close to ($\varepsilon_{ad}/\varepsilon_{\mathrm{v}} = 99.99\%$) the lower edge of the band gap of the photonic crystal, respectively.

After the laser fields are turned on, the population densities of the atomic levels exhibit Rabi oscillations. Eventually, the oscillations are observed to stabilize and the level populations reach a steady state.

It can be seen from the transient plots in figures 3(a) and (b) that the steady-state population densities ρ_{aa} and ρ_{dd} decrease as the resonance energy ε_{ad} approaches the lower band edge.

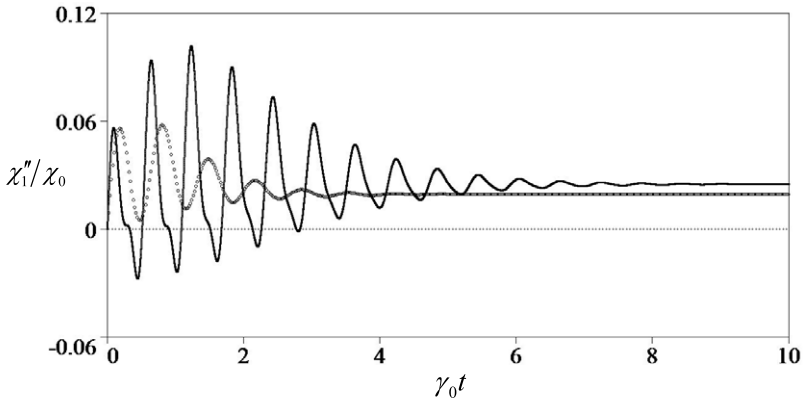

Figure 4. Numerical plots of the time evolution of χ_1''/χ_0 for $\varepsilon_{ad}/\varepsilon_v = 80.00\%$ (solid curve) and $\varepsilon_{ad}/\varepsilon_v = 99.99\%$ (dotted curve), using the atomic scheme in figure 1(a). All other resonance energies are kept away from either of the band edges at all times. The horizontal axis shows scaled time $\gamma_0 t$.

On the other hand, as seen in the plots in figures 3(c) and (d), the population densities ρ_{bb} and ρ_{cc} have higher steady-state values under the same scenario. This is a very interesting behaviour which has not been studied previously in this system. The explanations behind these observations are given below.

With increasing proximity of the resonance energy ε_{ad} to the lower band edge, the decay rate Γ_a given in equation (7*a*) becomes larger due to the growing value of the form factor (see figure 2). A larger value of Γ_a has the effect of depopulating level $|a\rangle$ with increasing rapidity, as seen from equation (6*a*). This, in turn, leads to a substantial decline in the steady-state level population ρ_{aa}.

Using equation (6*d*) and assuming steady-state conditions, the population density ρ_{dd} can be written as $\rho_{dd} = (\Gamma_a \rho_{aa})/\Gamma_d$. This indicates that ρ_{dd} is directly proportional to both Γ_a and ρ_{aa}. Although the decay rate Γ_a increases as the resonance energy ε_{ad} approaches the lower band edge, the range of its values remain within the same order of magnitude. In contrast, for the same change in the resonance energy, the decrease in ρ_{aa} is over several orders of magnitude as it is proportional to an exponentially decaying function of Γ_a. Consequently, ρ_{dd} is observed to decrease.

The reason behind the increase in the steady-state population density ρ_{cc} is its dependence on ρ_{dd}, as seen from equation (6*c*). Since level $|d\rangle$ decays to level $|c\rangle$, a decrease in ρ_{dd} implies an increase in ρ_{cc}. Similarly, the steady-state population density ρ_{bb} is observed to increase as ε_{ad} approaches the band edge. This is due to the fact that an increase in the population in level $|c\rangle$ means that more particles are pumped up to level $|b\rangle$, as seen from the last term on equation (6*b*). It is worthwhile noting that this effect is also expected in the case of level $|e\rangle$, although to a much smaller degree (not plotted).

The most important result concerning the steady-state level populations is obtained from figure 3(d). It can be seen that, as ε_{ad} approaches the band edge, an inversion occurs in the population density of the ground level $|c\rangle$. Therefore, it is possible to switch the system from an inverted state to a non-inverted state (and vice versa), with respect to level populations, by manipulating the resonance energy between levels $|a\rangle$ and $|d\rangle$. This is a very significant new finding of our theory, which can be used to make new types of photonic switches.

Figure 4 shows the time evolution of χ_1''/χ_0 for the atom in figure 1(a), at resonance energies away (solid curve) and close (dotted curve) to the band edge. The curves are drawn

using the same detuning parameters and probe field strength as in figure 3. The Rabi frequencies of the pump fields in this case are $\Omega_\alpha/\gamma_0 = \Omega_\beta/\gamma_0 = 15$. Due to the relatively large values of these frequencies, one can now see a greater number of oscillations. A similar set of values for these Rabi frequencies will be used later in our analyses of the system in the steady state.

In figure 4, it is interesting to note that, as ε_{ad} approaches the band edge and the decay rate Γ_a increases, χ_1''/χ_0 reaches its steady-state value comparatively earlier and with fewer oscillations (see dotted curve). This can be understood by considering the fact that χ_1''/χ_0 depends on the level population ρ_{cc}, which attains steady state earlier for large values of Γ_a (see equation (6*n*) and figure 3(d)).

Finally, with regards to the transient calculations presented above, it must be noted that similar results can also be obtained for the second atomic scheme given in figure 1(b).

Next, we present an analysis of the ac Stark effect in the doped atoms and study how it is affected by the band structure of the photonic crystal. The absorption profiles of the probe beams for the two atomic configurations in figure 1 have been calculated in figures 5 and 6, using equations (8*b*) and (16*b*), respectively. The Rabi frequencies in this case are: $\Omega_\alpha/\gamma_0 = \Omega_\beta/\gamma_0 = 10$ and $\Omega_p/\gamma_0 = 0.2$. The larger Rabi frequencies for the pump fields have been chosen to make the splitting effect more pronounced. For figures 5(a) and 6(a), the pump fields are considered to be resonant, i.e. $\Delta_{ab}/\gamma_0 = \Delta_{bc}/\gamma_0 = 0$, whereas in figures 5(b) and 6(b), $\Delta_{ab}/\gamma_0 = 2$ and $\Delta_{bc}/\gamma_0 = 0$. These parameters are similar to those used in [21]. As before, the solid and dash–dotted curves in figures 5 and 6 correspond to the cases when $\varepsilon_{ad}/\varepsilon_v = 80.00\%$ and $\varepsilon_{ad}/\varepsilon_v = 99.99\%$, respectively.

In figure 5, one can see that the absorption profiles represented by the two solid curves are each characterized by three peaks. This is an evidence of ac Stark splitting (dynamic) in this system. The mechanism that gives rise to this effect is briefly explained below.

When ε_{ad} lies away from the band edge of the crystal, we have the condition where the linewidth Γ_a is small compared to the Rabi frequencies Ω_α and Ω_β. In this situation, we get strong atom–field coupling and the dressed state of the system, which is a linear combination of the states $|a\rangle$, $|b\rangle$ and $|c\rangle$, splits into three states. As a result, one can now observe three transitions from the ground level $|c\rangle$ to the excited level $|e\rangle$ (see solid curves in figure 5). This splitting of energy levels has also been clearly explained using the idea of dressed states in [21], where similar results were obtained in atomic gases.

In both figures 5(a) and (b), as ε_{ad} approaches the band edge, the central peak disappears and the heights of the two side peaks increase (dash–dotted curves). In addition, one can observe shifts in the locations of the side peaks. These are very interesting observations which have not been made previously in this system.

The disappearance of the central peak can be explained as follows. In the presence of strong pump field Rabi frequencies Ω_α and Ω_β, the system has three dressed states, as mentioned before. Note that the three peaks in figure 5(a) are located at $\Delta_{ec}/\gamma_0 = -\frac{1}{2\gamma_0}\sqrt{\Omega_\alpha^2 + \Omega_\beta^2} \approx -7.07$, $\Delta_{ec}/\gamma_0 = 0$ and $\Delta_{ec}/\gamma_0 = \frac{1}{2\gamma_0}\sqrt{\Omega_\alpha^2 + \Omega_\beta^2} \approx 7.07$ (solid curve in figure 5(a)).

When the resonance energy lies near the band edge, $\Gamma_a \geqslant \Omega_\alpha$ and the effect of Ω_α disappears. In other words, the effect of the pump field with Rabi frequency Ω_α is inhibited by the band structure of the photonic crystal. Now the system has two dressed states which are a linear combination of states $|b\rangle$ and $|c\rangle$. As a result, we get two transitions located at $\Delta_{ec}/\gamma_0 = -\Omega_\beta/(2\gamma_0) = -5$ and $\Delta_{ec}/\gamma_0 = \Omega_\beta/(2\gamma_0) = 5$.

Similar explanations are applicable to the dash–dotted curve in figure 5(b), except the locations and the relative heights of the peaks will be different owing to the non-zero detuning parameter Δ_{ab}/γ_0.

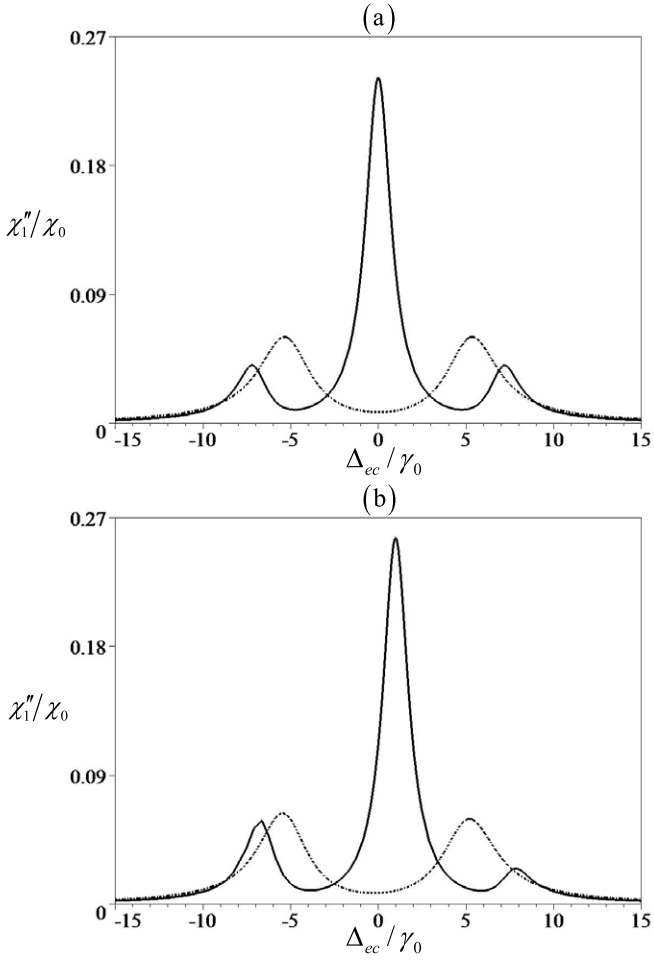

Figure 5. Plots of χ_1''/χ_0 against probe field detuning Δ_{ec}/γ_0 for the atom in figure 1(a), in steady state. In (a) $\Delta_{ab}/\gamma_0 = \Delta_{bc}/\gamma_0 = 0$ and in (b) $\Delta_{ab}/\gamma_0 = 2$ and $\Delta_{bc}/\gamma_0 = 0$. The Rabi frequencies of the laser fields are taken as $\Omega_\alpha/\gamma_0 = \Omega_\beta/\gamma_0 = 10$ and $\Omega_p/\gamma_0 = 0.2$. The solid curves are drawn for the case where all resonance energies are away from either of the band edges and $\varepsilon_{ad}/\varepsilon_v = 80.00\%$. The dash–dotted curves represent the case where $\varepsilon_{ad}/\varepsilon_v = 99.99\%$ while all other energies remain far from the band edges.

In figure 6, we have plotted the imaginary part of the susceptibility for the atomic configuration in figure 1(b), where the probe field sweeps the $|b\rangle \rightarrow |e\rangle$ transition. For figure 6(a), both the pump fields are considered to be resonant, whereas for figure 6(b) the pump field with Rabi frequency Ω_α has non-zero detuning. When ε_{ad} lies away from the band edge, one can see that the absorption profile seen in the solid curve in figure 6(a) is characterized by two strong peaks. In contrast, in figure 6(b), the solid curve has three peaks. However, as the resonance energy approaches the band edge of the crystal, we observe two peaks for each of the plots in figure 6 (dash–dotted curves) and the locations of the peaks shift towards the zero detuning mark.

In order to understand the effect in figure 6(a), we recall that the system can have three dressed states due to the strong coupling of the pump fields. If both pump fields are resonant, the transition from the middle dressed state is forbidden. In this case, the location of the peaks

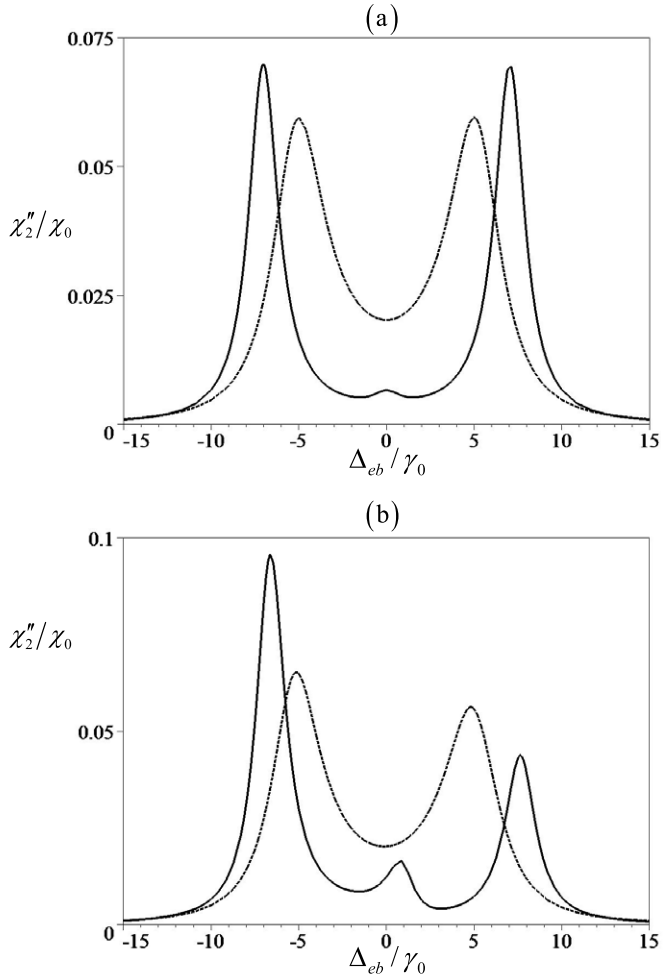

Figure 6. Plots of χ_2''/χ_0 against probe field detuning Δ_{eb}/γ_0 for the atom in figure 1(b), in steady state. In (a) $\Delta_{ab}/\gamma_0 = \Delta_{bc}/\gamma_0 = 0$ and in (b) $\Delta_{ab}/\gamma_0 = 2$ and $\Delta_{bc}/\gamma_0 = 0$. The Rabi frequencies of the laser fields are taken as $\Omega_\alpha/\gamma_0 = \Omega_\beta/\gamma_0 = 10$ and $\Omega_p/\gamma_0 = 0.2$. The solid curves are drawn for the case where all resonance energies are away from either of the band edges and $\varepsilon_{ad}/\varepsilon_v = 80.00\%$. The dash–dotted curves represent the case where $\varepsilon_{ad}/\varepsilon_v = 99.99\%$ while all other energies remain far from the band edges.

are $\Delta_{eb}/\gamma_0 = -\frac{1}{2\gamma_0}\sqrt{\Omega_\alpha^2 + \Omega_\beta^2} \approx -7.07$ and $\Delta_{eb}/\gamma_0 = \frac{1}{2\gamma_0}\sqrt{\Omega_\alpha^2 + \Omega_\beta^2} \approx 7.07$. When the resonance energy lies near the band edge and the decay rate Γ_a is large compared to Ω_α we get two transitions located at $\Delta_{eb}/\gamma_0 = -\Omega_\beta/2 = -5$ and $\Delta_{eb}/\gamma_0 = \Omega_\beta/2 = 5$.

Figure 6(b) can be explained in a similar way to figure 5(b). It can also be seen from this figure that the central peak is significantly weaker than the side peaks. This can be explained by the fact that, at zero detuning, the transition from the middle state of the three dressed states of the system is forbidden (see discussion above). As the detuning is increased, the transition from the middle state becomes allowed. The dash–dotted curve in figure 6(b) can be explained in the same manner as that in figure 6(a), except the location of the peaks will be different due to the non-zero Δ_{ab}/γ_0 parameter.

In figures 5 and 6 we have shown that due to the role played by the band structure of the photonic crystal, the doped atom effectively becomes transparent to any radiation field tuned to the resonance energy of the probed transition. In fact, we have demonstrated that it is possible to switch from an absorption state to a non-absorption state (and vice versa) for the atomic system, by controlling the resonance energy. More precisely, the transparency is seen to be directly dependent on the location of the resonance energy with respect to the band gap of the crystal. This is a very important new finding as techniques of rendering material systems transparent to resonant laser radiation are very desirable for applications in quantum optics and radiation physics. For example, the transparency effect can be used to enhance the properties and efficiency of physical processes such as nonlinear frequency conversion, optical phase conjugation, squeezed-light generation, low-light-level photonic switching, etc [38].

A survey of relevant studies reveals that the most common techniques employed in producing the transparency effect include the manipulation of atomic response through adjustment of the intensity-ratio of pump fields [15, 22, 23], changing the amplitude and phase of the driving field(s) [16], tuning the pump field [39], etc. In the calculations presented in this work, a new technique for obtaining transparency has been shown, making use of the unique properties of the band structure of photonic crystals. This has great potential for applications in creating new photonic devices for quantum computing.

In the present paper we have studied the ac Stark effect caused by two external strong pump fields in a photonic crystal doped with five-level nanoparticles. The transparency obtained in our theory is an effect of the two pump fields and the decay rate due to the coupling between the atoms and the photonic crystal. There have been many other studies of transparency and splitting of energy levels in doped photonic crystals using systems and methods which are different from those considered in our paper. For example, Petrosyan and Kurizki [40] have studied four-level atoms where they have applied a probe and a pump field. They observed EIT and the splitting effect due to the coupling of the atom to the localized DOS and the DOS at the band edge of the crystal. Similar studies have also been performed by other researchers [41]. In contrast to these works, we do not consider the A–T splitting of the resonance energy due to the coupling of the transition to the DOS. Instead, the splitting effect demonstrated in our paper occurs due to the external laser fields. This is a very important distinction.

EIT has also been achieved by Singh in four-level atoms doped in a photonic crystal with the application of only one laser field [35]. It is found that the medium can be transformed from a transparent to a non-transparent state just by changing the location of the resonance energy. More recently, induced transparencies in photonic crystals have been studied using cross-phase modulation [42]. The EIT effect in spontaneous emission has also been investigated in a double-band photonic crystal doped with both V-type three-level and double V-type four-level atoms [43].

The isotropic model of the photonic crystal leads to a divergent DOS at the band edge [27, 28, 30, 44]. It is important to specify how far from the divergent band edge the resonance energy needs to be in order to facilitate the Markovian approximation. Analyses of the decay of an atom with the resonance energy close to the band edge energy have shown that the band edge modes behave like a cavity and the atom–band edge modes interaction splits the atomic resonance into a doublet [31]. One component of the doublet falls in the continuum of states and decays. The other component falls inside the band gap giving rise to a photon–atom bound state. The magnitude of the splitting is a function of atom–band edge detuning. For some values of this detuning, the splitting disappears or its influence on the atom becomes negligible.

If the atomic frequency is inside the band gap, the isotropic model guarantees the existence of an atom–photon bound state. This becomes evident through oscillations in the atomic

inversion. However, in the present paper, we have not considered the case where the resonance energy lies in the band gap. Instead, we have taken the resonance energy to be within the band but not at the band edge. It is important to note that for large detunings from the band edge, the magnitude of the oscillations in the atomic inversion becomes negligibly small [27].

It is known that the typical signature of non-Markovian effects [27, 28, 30, 44] is a non-exponential decay [27, 45]. It can be deduced from [27, 45] that, in the isotropic photonic crystal considered in our paper, the Markovian approximation is valid if the detuning $\Delta\varepsilon \equiv \varepsilon_{\mathrm{v}} - \varepsilon_{ad}$ approximately satisfies the following condition:

$$\frac{|\Delta\varepsilon|}{\varepsilon_{\mathrm{v}}} \geqslant \frac{50\beta_{\mathrm{I}}}{\varepsilon_{\mathrm{v}}} \tag{19}$$

where β_{I} is defined as the characteristic energy of the atom–photon interaction [27]. In other words, the Markovian approximation is valid when the DOS can be considered smooth on the scale determined by this characteristic energy. β_{I} can be approximated as [27, 45]:

$$\beta_{\mathrm{I}} = \left[\frac{\sqrt{\pi/A_{\mathrm{I}}}(\varepsilon_{ad}\mu_{ad})^2}{12\sqrt{\hbar}\epsilon_0\varepsilon_{\mathrm{v}}L^2}\right]^{2/3} \tag{20}$$

with the constant A_{I} obtained using the energy dispersion relation given in equation (1) as [31]:

$$A_{\mathrm{I}} = \left[-\frac{cL^2}{2a(1+n)^2\sin(4na\varepsilon_{\mathrm{v}}/c\hbar)}\right]. \tag{21}$$

Putting the above equation into β_{I}, we get:

$$\beta_{\mathrm{I}} = \left(\frac{(\varepsilon_{ad}\mu_{ad})^2}{12\sqrt{\hbar}\epsilon_0\varepsilon_{\mathrm{v}}L^2}\right)^{2/3}\left[-\frac{2a\pi(1+n)^2\sin(4na\varepsilon_{\mathrm{v}}/c\hbar)}{cL^2}\right]^{1/3}. \tag{22}$$

Using equations (19) and (22), we found that:

$$\frac{|\Delta\varepsilon|}{\varepsilon_{\mathrm{v}}} \geqslant 10^{-5}. \tag{23}$$

In our paper, the largest value of ε_{ad} gives:

$$\frac{|\Delta\varepsilon|}{\varepsilon_{\mathrm{v}}} = \frac{(\varepsilon_{\mathrm{v}} - 0.9999\varepsilon_{\mathrm{v}})}{\varepsilon_{\mathrm{v}}} = 10^{-4}. \tag{24}$$

Therefore, from the above calculations, we conclude that the Markovian approximation performs relatively well.

Finally, it is interesting to note that the formalism and results obtained for the isotropic model also apply to one-dimensional systems. This can be very advantageous as one-dimensional systems can be implemented as waveguide channels in real three-dimensional photonic crystals [46].

In summary, we have studied the time evolution of the level populations and both the transient and the steady-state behaviours of the imaginary part of the susceptibility in an isotropic photonic crystal doped with doubly-driven five-level atoms. We found that manipulation of the decay rate offers a new mechanism for switching the atomic system from an inverted to a non-inverted state (and vice versa), with regards to the level population of the ground state of the atom. We have also performed numerical simulations for the imaginary part of the susceptibility. Our calculations have shown that due to the role played by the band structure of the photonic crystal, the doped atom effectively becomes transparent to any radiation field tuned to the resonance energy of the probed transition. Therefore, it is possible to switch between an absorption state and a non-absorption state of the atomic system by controlling the resonance energy. This is a very important finding as techniques of rendering material systems transparent to resonant laser radiation are very desirable for applications in quantum optics and radiation physics.

Acknowledgments

The authors are grateful to Dr Marian Florescu for helpful discussions. MRS wishes to thank the Natural Sciences and Engineering Research Council (NSERC) of Canada for financial support in the form of a research grant. IH is grateful to the NSERC for a postgraduate scholarship.

References

[1] Arimondo E 1996 *Progress in Optics* vol 35, ed E Wolf (Amsterdam: Elsevier Science) chapter 5
Marangos J P 1998 *J. Mod. Opt.* **45** 471
Lukin M D 2003 *Rev. Mod. Phys.* **75** 457
[2] Harris S E 1989 *Phys. Rev. Lett.* **62** 1033
Narducci L M, Doss H M, Ru P, Scully M O, Zhu S-Y and Keitel C 1991 *Opt. Commun.* **81** 379
Mompart J and Corbalán R 2000 *J. Opt. B: Quantum Semiclass. Opt.* **2** R7
Kocharovskaya O A, Matsko A B and Rostovtsev Y 2002 *Phys. Rev.* A **65** 013803
[3] Boller K-J, Imamoğlu A and Harris S E 1991 *Phys. Rev. Lett.* **66** 2593
Harris S E 1997 *Phys. Today* **50** 36
Bentley C L Jr, Liu J and Liao Y 2000 *Phys. Rev.* A **61** 023811
Fleischhauer M, Imamoğlu A and Marangos J P 2005 *Rev. Mod. Phys.* **77** 633
[4] Scully M O 1991 *Phys. Rev. Lett.* **67** 1855
Harris S E, Field J E and Kasapi A 1992 *Phys. Rev.* A **46** R29
Szymanowski C and Keitel C H 1994 *J. Phys. B: At. Mol. Opt. Phys.* **27** 5795
Zibrov A S, Lukin M D, Hollberg L, Nikonov D E, Scully M O, Robinson H G and Velichansky V L 1996 *Phys. Rev. Lett.* **76** 3935
[5] Autler S H and Townes C H 1955 *Phys. Rev.* **100** 703
Cohen-Tannoudji C and Reynaud S 1977 *J. Phys. B: At. Mol. Phys.* **10** 345 and references therein
Delone N B and Kraĭnov V P 1999 *Phys. Usp.* **42** 669 and references therein
[6] Schabert A, Keil R and Toschek P E 1975 *Opt. Commun.* **13** 265
[7] Mollow B R 1972 *Phys. Rev.* A **5** 1522
[8] Delsart C and Keller J-C 1976 *J. Phys. B: At. Mol. Phys.* **9** 2769
Bjorkholm J E and Liao P F 1977 *Opt. Commun.* **21** 132
Gray H R and Stroud C R Jr 1978 *Opt. Commun.* **25** 359
Fisk P T H, Bachor H-A and Sandeman R J 1986 *Phys. Rev.* A **34** 4762
Jakob M and Kryuchkyan G Y 1998 *Phys. Rev.* A **57** 1355
[9] He X-F, Fisk P T H and Manson N B 1992 *J. Appl. Phys.* **72** 211
Yi P, Song M, Liu Y, Field R W, Li L and Lyyra A M 2004 *Opt. Commun.* **233** 131
[10] Teo B K, Feldbaum D, Cubel T, Guest J R, Berman P R and Raithel G 2003 *Phys. Rev.* A **68** 053407
Garcia-Fernandez R, Ekers A, Klavins J, Yatsenko L P, Bezuglov N N, Shore B W and Bergmann K 2005 *Phys. Rev.* A **71** 023401
[11] von Zanthier J, Skornia C, Agarwal G S and Walther H 2000 *Phys. Rev.* A **63** 013816
Sherman J A, Koerber T W, Markhotok A, Nagourney W and Fortson E N 2005 *Phys. Rev. Lett.* **94** 243001
[12] Girard B, Sitz G O, Zare R N, Billy N and Vigué J 1992 *J. Chem. Phys.* **97** 26
Xu S, Sha G, Jiang B, Sun W, Chen X and Zhang C 1994 *J. Chem. Phys.* **100** 6122
Qi J, Lazarov G, Wang X, Li L, Narducci L M, Lyyra A M and Spano F C 1999 *Phys. Rev. Lett.* **83** 288
[13] Shimano R and Kuwata-Gonokami M 1994 *Phys. Rev. Lett.* **72** 530
Tavares C J M, Costa Neto M A, Sitters R, Manson N B and Glasbeek M 1994 *Phys. Rev.* B **50** 13795
Qi J, Lazarov G, Wang X, Li L, Narducci L M, Lyyra A M and Spano F C 1999 *Phys. Rev. Lett.* **83** 288
[14] Bai Y S, Mossberg T W, Lu N and Berman P R 1986 *Phys. Rev. Lett.* **57** 1692
Qamar S, Zhu S-Y and Zubairy M S 2003 *J. Opt. B: Quantum Semiclass. Opt.* **5** 175
[15] McGloin D 2003 *J. Phys. B: At. Mol. Opt. Phys.* **36** 2861
[16] Hua X-M, Xiong J and Peng J-S 2001 *Eur. Phys. J.* D **13** 401
[17] Bimberg D, Grundmann M and Ledentsov N N 1999 *Quantum Dot Heterostructures* (Chichester: Wiley)
Harrison P 2005 *Quantum Wells, Wires and Dots* (Chichester: Wiley)
[18] Barenco A, Deutsch D, Ekert A and Jozsa R 1995 *Phys. Rev. Lett.* **74** 4083
Bayer M, Stern O, Hawrylak P, Fafard S and Forchel A 2000 *Nature* **405** 923
Michler P, Imamoğlu A, Mason M D, Carson P J, Strouse G F and Buratto S K 2000 *Nature* **406** 968

Kamada H, Gotoh H, Temmyo J, Takagahara T and Ando H 2001 *Phys. Rev. Lett.* **87** 246401
Regelman D V, Mizrahi U, Gershoni D, Ehrenfreund E, Schoenfeld W V and Petroff P M 2001 *Phys. Rev. Lett.* **87** 257401
Chow W W, Schneider H C and Phillips M C 2003 *Phys. Rev.* A **68** 053802
[19] Zhang T Y, Zhao W, Cao J C and Qasim G 2005 *J. Appl. Phys.* **98** 094311
Zhang T Y and Zhao W 2006 *Phys. Rev.* B **73** 245337
[20] Dynes J F, Frogley M D, Beck M, Faist J and Phillips C C 2005 *Phys. Rev. Lett.* **94** 157403
[21] Wei C, Suter D, Winsdor A S W and Manson N B 1998 *Phys. Rev.* A **58** 2310
[22] Narayanana A, Srinivasan R, Khan U K, Vudayagiri A and Ramachandran H 2004 *Eur. Phys. J.* D **31** 107
Narayanan A 2006 *Eur. Phys. J.* D **39** 13
[23] Sun J, Zuo Z, Mi X, Yu Z, Jiang Q, Wang Y, Wu L-A and Fu P 2004 *Phys. Rev.* A **70** 053820
[24] Chang W-H, Chen W-Y, Chang H-S, Hsieh T-P, Chyi J-I and Hsu T-M 2006 *Phys. Rev. Lett.* **96** 117401
Barth M, Schuster R, Gruber A and Cichos F 2006 *Phys. Rev. Lett.* **96** 243902 and references therein
[25] John S 1987 *Phys. Rev. Lett.* **58** 2486
Yablonovitch E 1987 *Phys. Rev. Lett.* **58** 2059
[26] Yablonovitch E, Gmitter T J and Leung K M 1991 *Phys. Rev. Lett.* **67** 2295
[27] Florescu M and John S 2001 *Phys. Rev.* A **64** 033801
[28] Vats N, John S and Busch K 2002 *Phys. Rev.* A **65** 043808
Florescu M and John S 2004 *Phys. Rev.* A **69** 053810
Toader O and John S 2005 *Phys. Rev.* E **71** 036605
Chan T Y M, Toader O and John S 2006 *Phys. Rev.* E **73** 046610
[29] Joannopoulos J D, Meade R D and Winn J N 1995 *Photonic Crystals* (Princeton, NJ: Princeton University Press)
Lourtioz J-M, Benisty H, Berger V, Gerard J-M, Maystre D, Tchelnokov A and Favennec P-N 2005 *Photonic Crystals: Towards Nanoscale Photonic Devices* (Berlin: Springer)
[30] John S and Quang T 1996 *Phys. Rev. Lett.* **76** 2484
Quang T, Woldeyohannes M, John S and Agarwal G S 1997 *Phys. Rev. Lett.* **79** 5238
Woldeyohannes M and John S 1999 *Phys. Rev.* A **60** 5046
Woldeyohannes M, John S and Rupasov V I 2001 *Phys. Rev.* A **63** 013814
Woldeyohannes M and John S 2003 *J. Opt. B: Quantum Semiclass. Opt.* **5** R43
[31] John S and Wang J 1990 *Phys. Rev. Lett.* **64** 2418
John S and Wang J 1991 *Phys. Rev.* B **43** 12772
[32] Rupasov V I and Singh M 1996 *Phys. Rev. Lett.* **77** 338
Rupasov V I and Singh M 1997 *Phys. Rev.* A **56** 898
[33] Rupasov V I and Singh M 1997 *Phys. Rev.* A **54** 3614
Singh M 2003 *J. Mod. Opt.* **50** 1319
Singh M and Haque I 2005 *J. Mod. Opt.* **52** 1857
[34] Singh M 2004 *Phys. Rev.* A **69** 023807
[35] Singh M 2004 *Phys. Rev.* A **70** 033813
[36] Ahmed E, Hansson A, Qi P, Kirova T, Lazoudis A, Kotochigova S, Lyyrab A M, Li L, Qi J and Magnier S 2006 *J. Chem. Phys.* **124** 084308
[37] Scully M O and Zubairy M S 1997 *Quantum Optics* (Cambridge: Cambridge University Press) chapter 7
[38] Boyd R W 2000 *IEEE J. Sel. Top. Quantum Electron.* **6** 881 and references therein
[39] Bhattacharyya D 2004 *J. Opt. B: Quantum Semiclass. Opt.* **6** 563
[40] Petrosyan D and Kurizki G 2001 *Phys. Rev.* A **64** 023810
[41] Kofman A G, Kurizki G and Sherman B 1994 *J. Mod. Opt.* **41** 353
John S and Quang T 1994 *Phys. Rev.* A **50** 1764
Paspalakis E, Kylstra N J and Knight P L 1999 *Phys. Rev.* A **60** R33
Du C, Hu Z and Li S 2004 *J. Opt. B: Quantum Semiclass. Opt.* **6** 263
[42] Bermel P, Rodriguez A, Johnson S G, Joannopoulos J D and Soljacic M 2006 *Phys. Rev.* A **74** 043818
[43] Zhang H Z, Tang S H, Dong P and He J 2002 *Phys. Rev.* A **65** 063802
[44] de Vega I, Alonso D and Gaspard P 2005 *Phys. Rev.* A **71** 023812
Mogilevtsev D, Kilin S, Cavalcanti S B and Hickmann J M 2005 *Phys. Rev.* A **72** 043817
Mogilevtsev D and Kilin S 2004 *Phys. Rev.* A **69** 053809
Mogilevtsev D, Kilin S and Cavalcanti S B 2004 *Photonics Nanostr.-Fund. Appl.* **2** 161
Mogilevtsev D, Kilin S and Cavalcanti S B 2005 *Photonics Nanostr.-Fund. Appl.* **3** 38
[45] Florescu M 2007 private communication
[46] Florescu M, Scheel S, Haeffner H, Lee H, Strekalov D, Knight P L and Dowling J P 2005 *Europhys. Lett.* **69** 945